

# Single amino acid insertion allows functional transduction of murine hepatocytes with human liver tropic AAV capsids

Marti Cabanes-Creus,<sup>1</sup> Renina Gale Navarro,<sup>1</sup> Sophia H.Y. Liao,<sup>1</sup> Grober Baltazar,<sup>1</sup> Matthieu Drouyer,<sup>1</sup> Erhua Zhu,<sup>2</sup> Suzanne Scott,<sup>2,3</sup> Clement Luong,<sup>1</sup> Laurence O.W. Wilson,<sup>3</sup> Ian E. Alexander,<sup>2,4</sup> and Leszek Lisowski<sup>1,5,6</sup>

<sup>1</sup>Translational Vectorology Research Unit, Children's Medical Research Institute, The University of Sydney, Westmead, NSW 2145, Australia; <sup>2</sup>Gene Therapy Research Unit, Children's Medical Research Institute and The Children's Hospital at Westmead, The University of Sydney, Westmead, NSW 2145, Australia; <sup>3</sup>Australian e-Health Research Centre, Commonwealth Scientific and Industrial Research Organisation (CSIRO), Sydney, NSW 2113, Australia; <sup>4</sup>Discipline of Child and Adolescent Health, Sydney Medical School, Faculty of Medicine and Health, The University of Sydney, Westmead, NSW 2145, Australia; <sup>5</sup>Vector and Genome Engineering Facility, Children's Medical Research Institute, The University of Sydney, Westmead, NSW 2145, Australia; <sup>6</sup>Military Institute of Medicine, Laboratory of Molecular Oncology and Innovative Therapies, 04-141 Warsaw, Poland

**Recent successes in clinical gene therapy applications have intensified the interest in using adeno-associated viruses (AAVs) as vectors for gene delivery into human liver. An inherent intriguing characteristic of AAVs is that vector variants vary substantially in their ability to transduce hepatocytes from different species. This has historically limited the value of preclinical studies using rodent models for predicting the efficiency of AAV vectors in liver-targeted gene therapy clinical studies. In this work, we aimed to investigate the key determinants of the observed differential interspecies transduction abilities among AAV variants. We took advantage of domain swapping strategies between AAV-KP1, a newly identified variant with enhanced murine liver tropism, and AAV3b, which functions poorly in mice. The systematic *in vivo* comparison of AAV3b/AAV-KP1 chimeric variants allowed us to identify a threonine insertion at position 265 within variable region I (VR-I) as the key residue that confers murine hepatic transduction to human-derived clade B (AAV2-like) and clade C (AAV3b-like) variants. We propose to use this insertion to generate phylogenetically related AAV surrogates in support of toxicology and dosing studies in the murine liver model.**

## INTRODUCTION

Adeno-associated viruses (AAVs), from which AAV vector systems were derived, have progressed into liver-directed gene therapy trials for both inborn errors of metabolism and hemophilia.<sup>1,2</sup> Novel AAV capsids, directly isolated from the human liver tissue or bioengineered, hold the promise of increasing the number of genetic diseases amenable for gene therapy in the coming years.<sup>3-6</sup>

An inherent intriguing characteristic of AAVs is that vector variants vary substantially in their ability to physically and functionally transduce (defined here as cell entry and transgene expression, respectively) hepatocytes from different species.<sup>7</sup> This has limited the value of studies using rodent and other animal models for predicting the

efficiency of AAV vectors in liver-targeted gene therapy clinical studies, hampering the preclinical development of novel human liver tropic capsids. Even though cumulative AAV transduction data from murine models reported by individual laboratories are consistent and widely accepted, the determinants of the interspecies transduction variability remain poorly understood.

For example, the non-human primate variants AAV7 (clade D) and AAV8 (clade E), as well as the human isolate AAV9 (clade F),<sup>8</sup> have been shown to perform well in the murine liver.<sup>9,10</sup> Since these viruses did not evolve to transduce murine hepatocytes, in this work, we depart from the premise that their performance in the murine liver is merely coincidental. Interestingly, these variants present a centrilobular transgene expression profile in the murine model,<sup>10</sup> which contrasts with the portal profile observed with AAV8 in cynomolgus and rhesus macaques.<sup>11</sup> Other variants, such as the bioengineered AAV-LK03<sup>6</sup> or the natural AAV2 or AAV3b (clade B/C), are known to function poorly in the murine liver.<sup>10</sup> More specifically, a post-entry deficiency has been suggested, with numerous reports highlighting a discrepancy between physical and functional transduction (FT) of these variants in the murine system (S. Tsuji et al., 2020, ASGCT conference).<sup>6,10</sup>

In this work, we aimed to investigate the key determinants of the observed differential interspecies transduction abilities among AAV variants. One of the most common methods used in AAV engineering involves the generation and subsequent selection of capsid libraries on the target cells. Of particular interest for this study are the libraries built using a DNA-family shuffling approach,<sup>12</sup> in which the output

Received 23 December 2020; accepted 21 April 2021;  
<https://doi.org/10.1016/j.omtm.2021.04.010>

**Correspondence:** Leszek Lisowski, Translational Vectorology Research Unit, Children's Medical Research Institute, The University of Sydney, 214 Hawkesbury Road, Westmead, NSW 2145, Australia.

**E-mail:** [llisowski@cmri.org.au](mailto:llisowski@cmri.org.au)



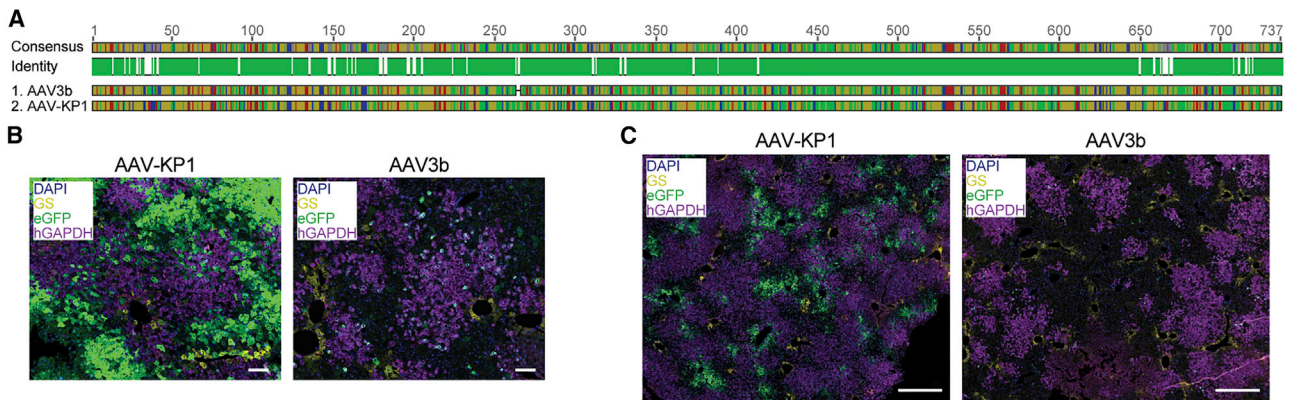


**Figure 1. Evaluation of AAV3b and AAV-KP1 in the humanized FRG (hFRG) model**

(A) VP1 pairwise sequence alignment of AAV3b and AAV-KP1. White vertical lines indicate diverging amino acids. The key amino acid for heparin interaction (R594) is common in AAV3b and AAV-KP1. Amino acid color scheme: yellow, non-polar; green, polar, uncharged; red, polar, acidic; blue, polar, basic. (B and C) Representative immunofluorescence analysis of hFRG chimeric mouse livers transduced with AAV3b and AAV-KP1. Scale bars, (B) 100  $\mu\text{m}$ , (C) 500  $\mu\text{m}$ . Purple indicates human GAPDH; yellow, glutamine synthetase (central vein); green, vector-expressed EGFP; and blue, DAPI (nuclei).

capsids are composed of fragments of the parental capsid that were included as inputs in the library preparation step. This process has historically yielded variants with new properties and enhanced tropism for targeted tissues, such as AAV-DJ, AAV-LK03, and AAV-NP59.<sup>3,6,12</sup> Importantly, those new AAV variants can also serve as powerful tools for understanding the function of individual capsid regions by enabling analysis of their individual contributions to the phenotypic profile of the final bioengineered variant. One of the latest examples of a novel variant selected from an AAV library is AAV-KP1,<sup>13</sup> a shuffled bioengineered capsid with improved tropism for human pancreatic islets.

Of interest, AAV-KP1 shares high sequence identity with the human tropic AAV3b (57 aa differences) and, similarly to the bioengineered variant AAV-LK03, it harbors the heparin-binding motif of AAV3b.<sup>14</sup> In marked contrast with AAV3b, AAV-KP1 has been reported to transduce both mouse and human hepatocytes in a xenograft mouse model of the human liver, the *Fah*<sup>-/-</sup>/*Rag2*<sup>-/-</sup>/*Il2rg*<sup>-/-</sup> (FRG),<sup>15</sup> positioning it as a potential genetic tool to determine the capsid regions responsible for murine transduction. Using domain swapping strategies between AAV-KP1 and AAV3b, we have determined that the insertion of threonine at capsid position 265 (Ser264\_Gly265insThr, referred throughout the manuscript as 265insT) is a key determinant for the enhanced functional performance of AAV-KP1 in murine hepatocytes, an effect independent of HSPG binding. Importantly, when moved into the otherwise human tropic AAV variants of clade B/C, we found this insertion in the variable region I (VR-I)<sup>16</sup> to significantly enhance entry and expression in murine hepatocytes. However, this came at the cost of reducing relative entry into human hepatocytes when tested in the humanized FRG (hFRG) mouse model of the human liver.

This work highlights VR-I as a critical player in the observed differential interspecies transduction of AAV variants. Furthermore, it

offers the possibility to generate murine-tropic, phylogenetically related surrogates of otherwise highly human hepatotropic AAV variants, supporting preclinical studies in murine models of the human liver.

## RESULTS

### AAV-KP1 and AAV3b transduce preferentially periportal hepatocytes, albeit with different preferences for murine and human hepatocytes

A recently identified bioengineered AAV variant, AAV-KP1,<sup>13</sup> shares high identity with the human isolate AAV3b, including its entire heparin-binding domain (HBD) (Figure 1A). To understand whether both variants use the same cell attachment mechanism, we first compared their heparin-binding affinities using a HiTrap heparin column. As shown in Table 1, both variants eluted at similar salt concentrations, indicating that AAV3b and AAV-KP1 have comparable affinities to heparin. This would indicate that the HBD that AAV-KP1 inherited from AAV3b dictates its attachment to heparan sulfate proteoglycan (HSPG). Next, we performed a functional evaluation of both variants in the hFRG xenograft model of the human liver. We injected intravenously  $2 \times 10^{11}$  vector genomes (vg)/mouse and evaluated reporter transgene expression in the chimeric liver 2 weeks after injection. Results presented in Figures 1B and 1C indicate that both variants exhibit a marked periportal transduction profile, regardless of the murine or human origin of the hepatocytes. In addition, and in marked contrast with AAV3b, we found that AAV-KP1 could transduce murine hepatocytes with high functional efficiency (Figures 1B and 1C). In contrast to previously published data,<sup>13</sup> AAV-KP1 was substantially more efficient at transducing murine hepatocytes than human hepatocytes (Figure 1C). These results suggest that the differential murine/human transduction is independent of HSPG binding and that one, or a combination, of the 57 aa that differ between AAV-KP1 and AAV3b unlocks AAV3b's functional transduction in murine hepatocytes.

**Table 1. Summary of HiTrap heparin column binding studies**

AAV capsid	AAV predominantly detected in:	[NaCl] at elution peak maxima (mM)
AAV3b	elution fraction	278.30
AAV-KP1	elution fraction	284.87
AAV3b-265insT	elution fraction	286.99
AAV-KP1-T265del	elution fraction	288.16
AAV-KP1-R595E-D599H	flow through	–
AAV-LK03	elution fraction	276.65
AAV-LK03-265insT	elution fraction	281.11
AAV-LK03-R594G	elution fraction	112.18
AAV-LK03-265insT-R595G	elution fraction	115.58

### Insertion of a threonine at position 265 unlocks murine hepatocyte transduction for AAV3b

Next, we aimed to elucidate which of the amino acids that differed between AAV-KP1 and AAV3b were responsible for the observed differences in the transduction of murine hepatocytes. To do so, we generated a subset of domain swaps and compared their performance in the murine liver *in vivo* using next-generation sequencing (NGS), including AAV-KP1 and AAV3b as references. Based on sequence clustering, we defined four differential regions between AAV-KP1 and AAV3b (Figure 2A). We subsequently built four AAV3b swaps that incorporated differential regions from AAV-KP1 (Figure 2A, swap1–4). Since the capsid region encompassing the HBD is shared between AAV-KP1 and AAV3b, it remained constant in the swapped AAV variants. To evaluate the individual swapped variants, we packaged five independently barcoded (BC) reporter constructs expressing EGFP under the control of a liver-specific promoter (LSP) (ssAAV-LSP1-EGFP-BC-WPRE-BGHpA) per variant. We subsequently titrated the individual vector preparations, and we mixed them at a 1:1:1 equimolar ratio. Finally, we injected the equimolar mix into a non-engrafted naive FRG mouse and harvested the liver cells 1 week post-injection. We subsequently extracted DNA and RNA/cDNA from the sorted cells, PCR-amplified the barcoded region of the transgene, deep-sequenced the amplicon, and mapped the barcodes to each capsid variant. This process is referred to throughout the manuscript as “barcoded NGS comparison.” Of particular interest is the expression index of the tested variants, which we define as the quotient of NGS reads mapped at the cDNA level and the reads mapped at the DNA level for each capsid.<sup>4</sup> The expression index allows comparison of AAV variants based on their ability to express the transgene at the mRNA level (functional transduction) following cell entry (physical transduction). As shown in Figure 2B, the only AAV3b-swapped variant able to functionally transduce murine hepatocytes was AAV3b-swap2, which harbors AAV-KP1 amino acid changes between positions 125 and 265 (Figure 2A; Table S1). We next performed an additional round of domain swapping, this time concentrating on region 2 only. Specifically, and as depicted in Figure 2A, we further divided AAV3b-swap2 into three mini-swaps

(referred to as mSwaps, Table S1). An additional barcoded NGS comparison allowed us to further narrow down the AAV-KP1 interest region to positions 224–265 (Figure 2C, AAV3b-mSwap3). We performed two additional swapping experiments (indicated in purple and orange in Figure 1A), which allowed us to determine that the key effect was maintained in AAV3b-Q263A+265insT (Figure 2D) and finally that the single insertion of a threonine at position 265 (VP1 numbering) was sufficient to substantially improve the functional performance of AAV3b in the murine liver (Figure 2E). Importantly, the original AAV3b's S264 and G265, which surround 265insT, are exposed to the capsid surface at the base of the protrusions of the 3-fold axis symmetry, although not in close proximity with the arginine (R594) key for HSPG attachment (Figure 2F). Given the shuffled nature of AAV-KP1, this variant is composed of regions of eight parental AAV capsids (AAV1, AAV2, AAV3b, AAV6, AAV8, AAV9, AAV-rh.10, and AAV-porcine-2). As detailed in Figure 2G, the region surrounding the threonine insertion at position 265 is of AAV1/6 origin.

### Threonine insertion at position 265 drives functional murine liver transduction for AAV3b and AAV1

We next validated the barcoded NGS comparison results by injecting individual AAV3b, AAV3b-265insT, AAV-KP1, and AAV-KP1-T265del vectors encoding identical ssAAV-LSP1-EGFP-WPRE-BGHpA expression cassettes into non-engrafted FRG mice (n = 3 FRG mice/variant). As shown in Figure 3A, the threonine insertion substantially improved functional transduction from AAV3b in the murine liver, although the zonation pattern remained periportal. Conversely, deletion of T265 in AAV-KP1 caused a substantial decrease in the expression potency of this variant (Figure 3A), although, again, the pattern of transduction remained unaltered (periportal). We subsequently evaluated the heparin-binding potency of AAV3b-265insT and AAV-KP1-T265del using a HiTrap heparin column. As presented in Table 1, we found that the insertion/deletion at position 265 did not have any significant effect on heparin binding, which, in agreement with our previously published results,<sup>4</sup> is consistent with the retention of a marked periportal transduction of these variants (Figure 3A). We next generated an HSPG de-targeted AAV-KP1 variant by introducing two point mutations at the capsid surface (R595E and D599H) aimed to reduce the interaction between AAV-KP1 and heparin. We confirmed the hypothesized reduction of heparin-binding strength using heparin affinity chromatography (Table 1). In marked contrast with AAV-KP1 (Figure 3A), the HSPG de-targeted AAV-KP1 variant lost its marked periportal profile (Figure 3B).

To obtain a more comprehensive picture of the functional differences between AAV3b and AAV3b-265insT, as well as functional differences between AAV-KP1 and its T265-deleted variant, we analyzed the vector copy number and the amount of GFP protein in liver lysate for each group of mice. We found the threonine insertion to substantially increase the physical transduction of AAV3b in the murine liver, as evident by an increase in vector genome copy number per diploid cell and GFP protein level in the total liver lysate (Figures 3C and 3D).

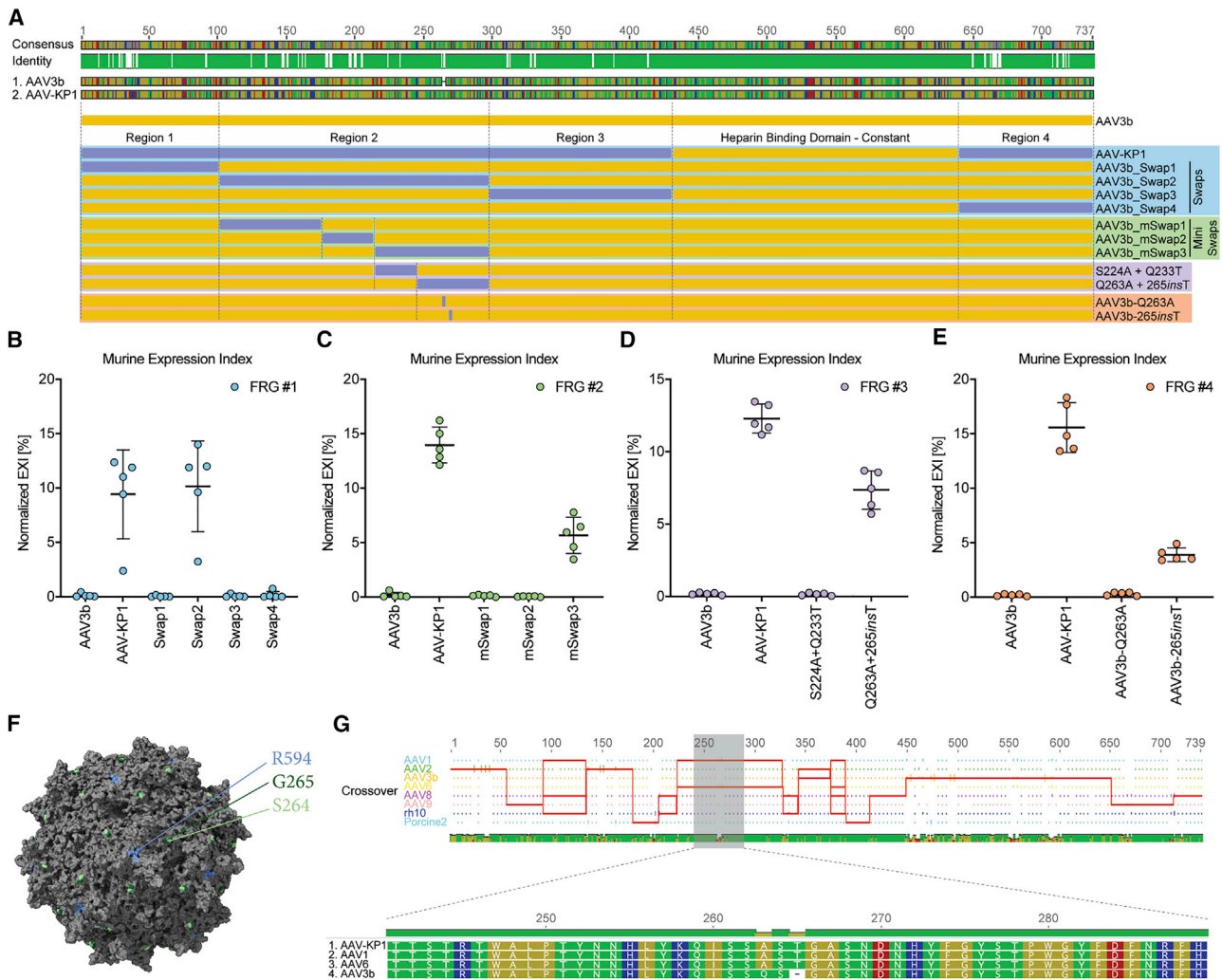


**Figure 2. Design and *in vivo* comparison of AAV3b variants harboring systematic swapped regions of AAV-KP1 origin**

(A) Schematic representation of AAV-KP1 regions (lavender) moved into the AAV3b scaffold (yellow). (B–E) *In vivo* comparison of AAV3b, AAV-KP1, and indicated swapped variants in non-engrafted FRG mice. The murine expression index corresponds to the quotient of the percentage of NGS reads mapped to each barcoded transgene at the cDNA level and the corresponding percentage at the DNA level ( $n = 5$  barcodes/capsid). Data are mean  $\pm$  SD (F) 3D map of the AAV3b capsid atomic model showing topological locations of the amino acids adjacent to 265insT displayed in green (S264, G265), and the key amino acid for heparin interaction displayed in blue (R594). (G) Parental sequence contribution analysis of AAV-KP1. The red line represents the most probable parental origin of each AAV-KP1 region based on the longest sequence of identity to parental variants in a 5' to 3' direction. Sequence identity between parental AAVs at each amino acid position is shown for reference (red, 0–0.3; yellow, at least 0.3 and less than 1; green, 1). The highlighted region surrounding the 265insT position on AAV-KP1, AAV1, AAV6, and AAV3b is shown in detail as a pairwise sequence alignment.

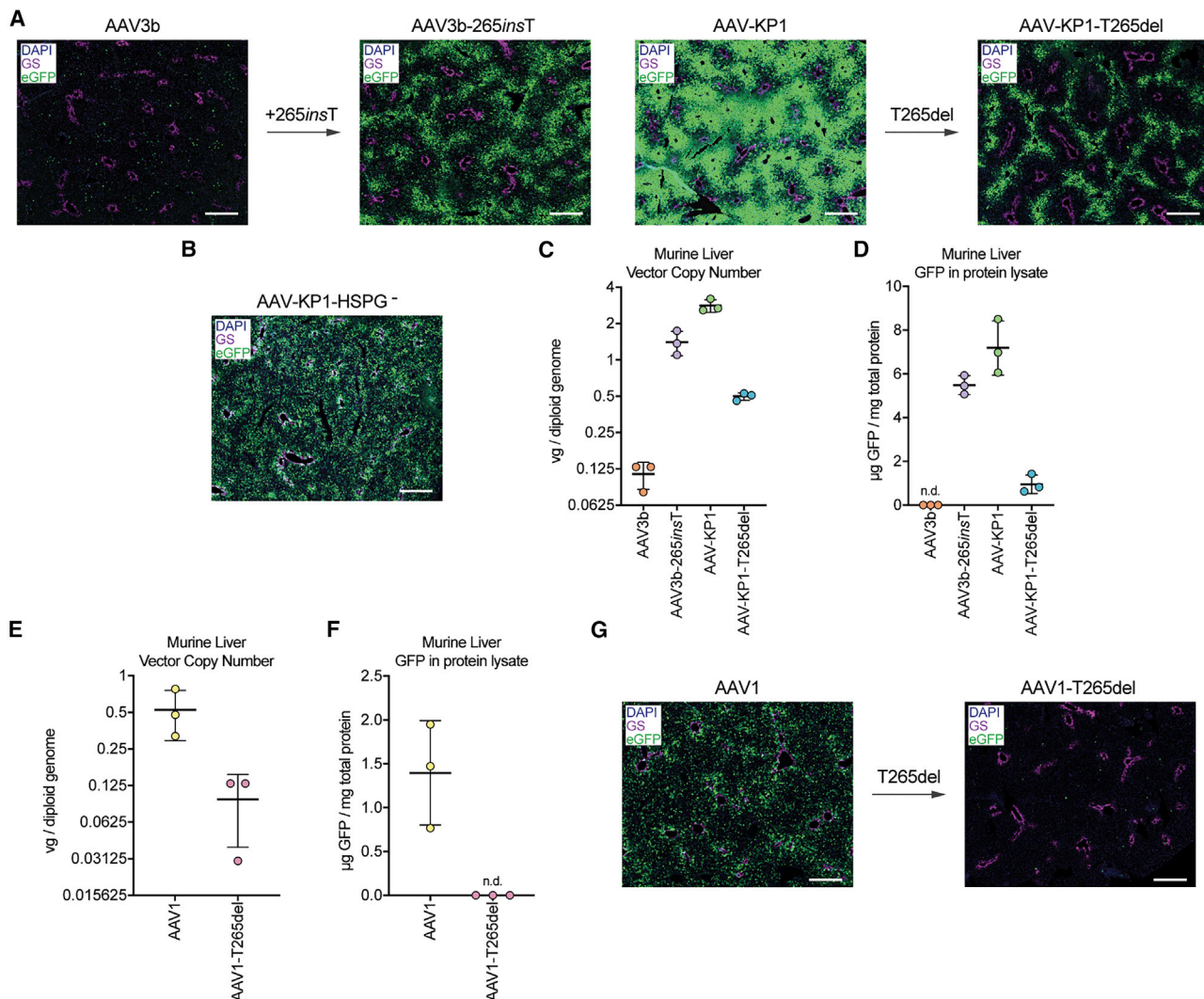
Conversely, we confirmed that the deletion of T265 in AAV-KP1 resulted in a marked decrease of vector transduction of this organ (Figure 3C), although this effect was even more pronounced at the functional level (Figure 3D).

Finally, given the AAV1 origin of 265insT, we tested the effect of deleting threonine 265 from this parental capsid. We compared the performance of AAV1 and AAV1-*T265del* in three non-engrafted FRG mice. Interestingly, we found this amino acid to be essential for AAV1's ability to functionally transduce murine liver, as shown by

a marked decrease in vg/diploid cell (Figure 3E),  $\mu$ g of GFP/mg of protein (Figure 3F), and immunofluorescence analyses of GFP expression in liver sections (Figure 3G).

#### Insertion of any amino acid at position 265 improves functional transduction of AAV3b in the murine liver

To evaluate whether the observed effect in the murine liver was specific to threonine (265insT) or to a general structural change due to the insertion of an amino acid, we generated an AAV3b-based saturation library harboring all 20 individual amino acids at position 265



(AAV3b-265insX). To compare the relative effects of these insertions to the canonical AAV3b (no insertion), we maintained AAV3b as part of the library pool. We evaluated the composition of the library at the plasmid level (Figure 4A), and at all subsequent stages using NGS of the region harboring the insertion. We cloned the plasmid library into a previously described replication-incompetent AAV selection platform, the functional transduction platform (Figure 4B).<sup>4</sup> This platform supports the recovery of capsid-encoding DNA molecules enclosed in the matching capsid and, importantly, of RNA transcripts driven by the native AAV p40 promoter (Figure 4B). All of the amino acid insertions, except for cysteine, were packaged with similar efficiency (Figures 4C and 4D). We injected three naive FRG mice

with  $5 \times 10^{10}$  total vg/mouse. One week post-injection, we recovered DNA and RNA from the murine liver and evaluated the relative performance of each variant at physical transduction (DNA, entry) and functional transduction (RNA/cDNA, expression) levels. Vector uptake is presented normalized to library composition (entry index) in Figure 4E. All amino acid insertions, except for cysteine, were found to either improve AAV3b uptake in the murine liver or to have a neutral effect. Interestingly, amino acids with negatively charged side chains (Asp, Glu) improved entry substantially, whereas amino acids with positively charged side chains (Arg, His, Lys) had a minimal effect on entry (Figure 4E). Consistent with the data presented before, the insertion effect was more evident at the functional

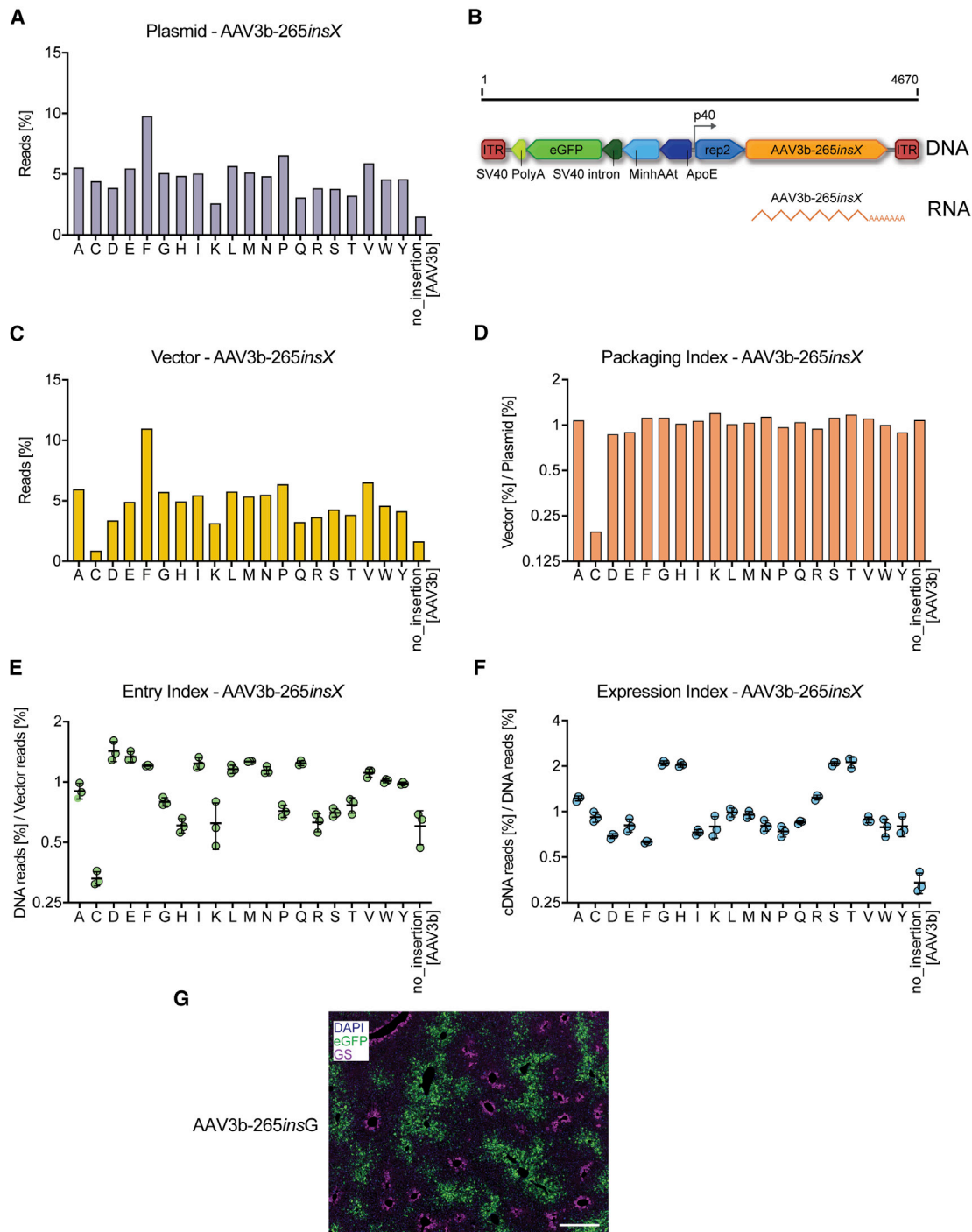


**Figure 4. Insertion of any amino acid at position 265 improves functional transduction of AAV3b in the murine liver**

(A) Amino acid composition of the library AAV3b-265insX at the plasmid level, expressed as the percentage of mapped NGS reads per variant. (B) Functional transduction (FT) selection platform. The capsid library is cloned downstream of the 3' *rep* region with the *cap* expression driven by the p40 promoter.<sup>4</sup> (C) Amino acid composition of the library AAV3b-265insX at the packaged vector level, expressed as percentage of mapped NGS reads per variant. (D) Packaging index expressed as the quotient between variant composition at the vector and at the plasmid levels. (E) Entry index expressed as the quotient between variant composition at the DNA recovered from the murine liver and variant composition at the vector level. (F) Expression index expressed as the quotient between variant composition at the cDNA and the DNA recovered from the murine liver. Data are mean  $\pm$  SD of three injected mice. (G) Representative immunofluorescence analysis of a FRG mouse liver transduced with AAV3b-265insG. Purple indicates glutamine synthetase (central vein); green, vector-expressed EGFP; and blue, DAPI (nuclei). Scale bar, 500  $\mu$ m.

transduction level (cDNA reads), where any amino acid insertion, including cysteine, led to a substantially higher level of expression when compared to AAV3b (Figure 4F). From all of the amino acids tested, this effect was more pronounced for glycine, histidine, serine, and the original threonine. We confirmed the NGS results by evaluating the performance of AAV3b-265*ins*G in naive FRG mice (Figure 4G).

#### Insertion of threonine at the structurally equivalent position in human tropic capsids improves entry to murine hepatocytes and expression in both species

Given the differences in preferential species transduction observed between AAV3b and AAV-KP1 (Figures 1B and 1C), we next evaluated the performance of AAV3b-265*ins*T and AAV-KP1-T265*del* in the hFRG model. As shown in Figure 5A, the insertion of threonine at position 265 in VR-I shifted transduction of AAV3b toward murine cells, whereas deletion of T265 in AAV-KP1 caused the contrary effect.

To study whether this effect was specific for AAV3b or translatable to other human-tropic AAV capsids, we introduced the threonine insertion at position 265 in the natural human liver isolates AAV-hu.Lvr05 and AAV-hu.Lvr06,<sup>5</sup> and in a bioengineered AAV2 variant with improved tropism for human hepatocytes in the hFRG mice (AAV2-N496D<sup>4</sup>). As observed in Figure 5B, the region surrounding VR-I is highly conserved between these variants and AAV-KP1, with the only exceptions of the key 265T insertion and the Q263A, which appears neutral for murine transduction (Figure 2E). To compare the variants with and without the threonine at position 265, we packaged barcoded expression cassettes into individual AAV variants and performed an NGS-based comparison ( $1 \times 10^{10}$  vg/capsid), as described earlier, in a naive FRG mouse. Figure 5C displays the average normalized reads mapped to each capsid in the non-engrafted mouse. We consistently found for all of the capsid variants tested that the insertion of threonine at position 265 substantially increased their murine liver transduction (Figure 5C). The insertion appeared to affect not only the entry but also the expression of the resultant variants. Importantly, this was consistent with AAV-KP1, where deletion of T265 resulted in a substantial loss in expression (Figure 5C). Next, we injected the same barcoded AAV mix into a hFRG mouse. We performed the barcoded comparison in murine liver cells and human hepatocytes by sorting the hepatocytes from each species 1 week post transduction. We found the read distribution in the murine liver highly comparable to that observed in non-engrafted mice (compare data in Figures 5D and 5C). As expected, based on the immunofluorescence results for AAV3b-265*ins*T (Figure 5A), the 265T insertion resulted in a marked relative decrease in human hepatocyte entry for all of the variants tested (Figure 5E). Deletion of 265T in AAV-KP1 caused, again, the opposite phenomenon (relative increase in human entry, Figure 5E). In the context of expression in human cells, the insertion seemed particularly effective in AAV3b, which achieved similar levels of RNA reads to AAV-KP1 (Figure 5E).

In order to confirm the NGS results, we injected  $n = 3$  non-engrafted naive FRG mice with AAV-hu.Lvr05, AAV-hu.Lvr06, AAV2-N496D,

and the corresponding variants with the 265T insertion. Representative images presented in Figure 5F show that the increase in murine transduction was also readily visible at the protein level, and it was especially apparent for AAV.hu.Lvr05 and AAV.hu.Lvr06, which at the dose tested did not transduce the murine liver with any appreciable efficiency ( $7.5 \times 10^{10}$  vg/capsid, Figure 5F, left panels). In agreement with the data presented earlier (Figure 5C), the insertion appeared to increase the entry of these variants in the murine liver (vector copy number, Figure 5G), which led to a substantial increase in EGFP protein levels in the liver lysate (Figure 5H).

Altogether, the 265 insertion appears to have two effects on capsid biodistribution in the chimeric hFRG model. First, variants harboring 265*ins*T display a stronger preference for physical transduction of murine hepatocytes over human hepatocytes (Figures 5D and 5E). Given the fixed amount of vector particles per injection, the results do not directly imply that the insertion hampers human entry, although this possibility cannot be excluded. Second, and perhaps more interesting from a capsid development perspective, the insertion appears to increase the transgene transcription levels, and this effect is observable in both murine and human hepatocytes, with the effects strikingly evident for the AAV3b-related capsids (Figures 5C–5E).

#### AAVR is an essential host factor for AAV3b-265*ins*T and AAV-KP1 functional transduction of HuH-7 cells

Interestingly, the VR-I loop, which is the site of the 265T insertion, has recently been observed in two cryogenic electron microscopy (cryo-EM) structures at the interface with the human AAV receptor (hAAVR).<sup>17–19</sup> We compared *in silico* the AAV-hAAVR interface between AAV1 (containing the 265T insertion) and AAV2 (Figure 6A). This analysis suggests that the insertion results in only a local distortion of the VR-I loop, with downstream residues S267/268, N268/269, D269/270, and N270/271 having similar C $\alpha$  positions in the AAV1-AAVR and AAV2-AAVR structures (Figure 6A). This is consistent with both AAV1 and AAV2 interacting with hAAVR, but at this point it is unclear whether this insertion would lead to a differential affinity for murine AAVR (mAAVR) and hAAVR.

Given the dependency of AAV3b on AAVR for functional transduction,<sup>17</sup> we next evaluated the net effect of 265T insertion in the human hepatoma-derived HuH-7 cell line. Interestingly, without the presence of confounding murine hepatocytes, we observed an increase in functional transduction for AAV3b-265*ins*T and a decrease for AAV-KP1-T265*del*, when compared to the respective parental variants on naive HuH-7 cells (Figure 6B). We observed no functional transduction of AAVR knockout (AAVR<sup>KO</sup>) HuH-7 cells (Figure 6C; Figure S1). Interestingly, and to our surprise, vector uptake remained unchanged when comparing these four vectors in HuH-7 and HuH-7 AAVR<sup>KO</sup> cells (Figures 6B and 6C). To study whether AAV-KP1 could still physically transduce HuH-7 cells with no AAVR, we performed a heparin competition assay (Figures 6D and 6E). Given the dependence of AAV-KP1 on HSPG for cell attachment, we supplemented soluble heparin (an analog of HSPG) in the media, which resulted in a decrease in functional transduction (GFP %) of HuH-7

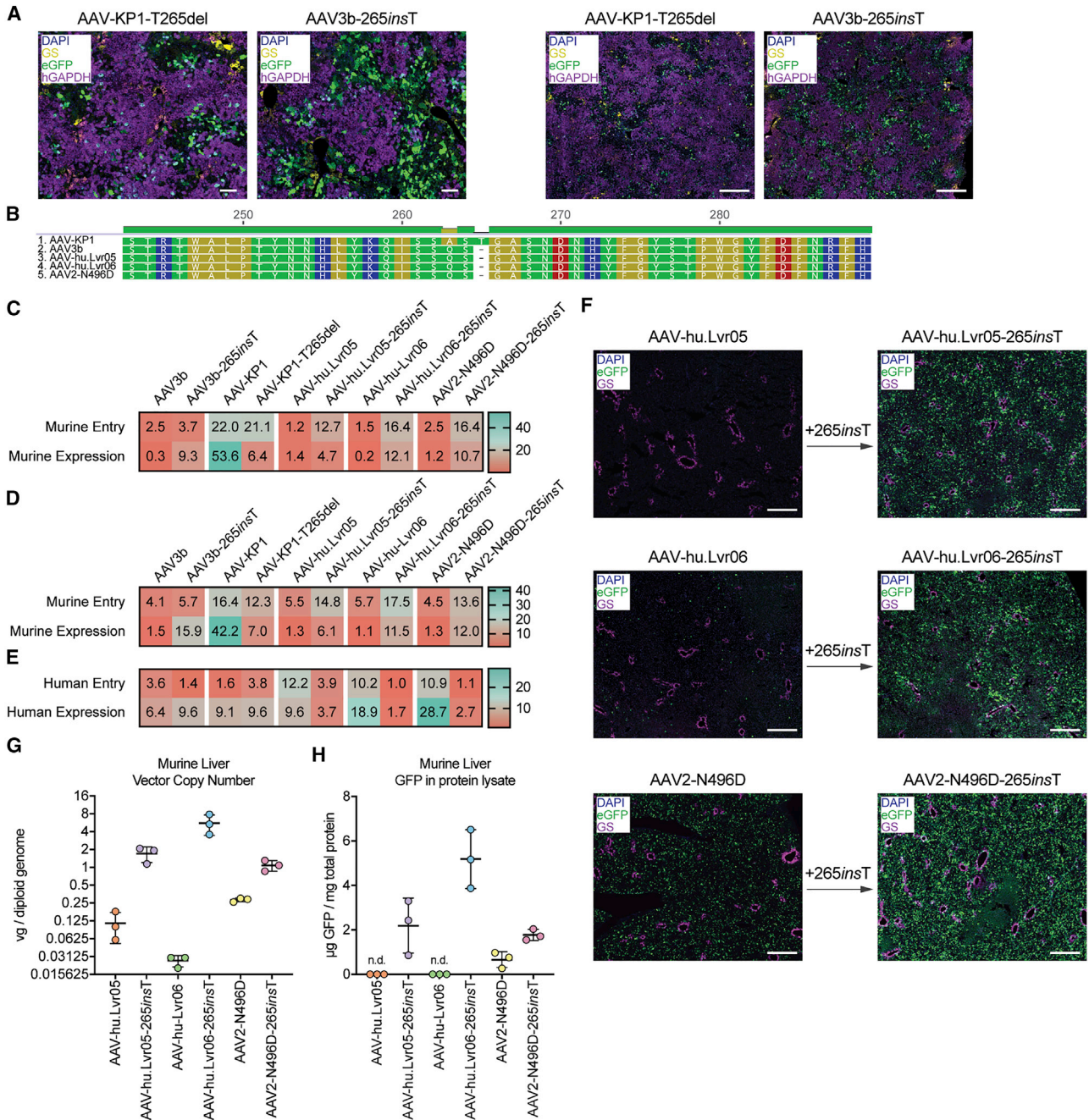


**Figure 5. *In vivo* comparison of 265T insertion/deletion AAV variants in hFRG mice**

(A) Representative immunofluorescence analysis of hFRG mouse livers transduced with AAV3b-265insT and AAV-KP1-T265del. Scale bars, left panel, 100  $\mu$ m; right panel, 500  $\mu$ m. Purple indicates human GAPDH; yellow, glutamine synthetase (central vein); green, vector-expressed EGFP; and blue, DAPI (nuclei). (B) VP1 pairwise sequence alignment of AAV-KP1, AAV3b, AAV-hu.Lvr05, AAV-hu.Lvr06, and AAV2-N496D. Region surrounding the 265insT is displayed (S243 to H289, AAV3b-VP1 numbering). (C) *In vivo* barcoded NGS comparison of indicated variants in a non-engrafted FRG mouse. Percentage of NGS reads mapped to each AAV variant (sum of  $n = 5$  barcodes/capsid) in the murine liver at the DNA (cell entry, physical transduction) and cDNA (expression, functional transduction) level, normalized to the pre-injection mix, is shown. (D and E) Barcoded NGS comparison of the same variants in a hFRG mouse. Normalized NGS reads mapped to each AAV variant in (D) murine liver cells and (E) human hepatocytes are shown. (F) Representative immunofluorescence analyses of FRG mice livers transduced with AAV-hu.Lvr05, AAV-hu.Lvr06, AAV2-N496D, and respective variants harboring the threonine insertion at position 265 (+265insT). Purple indicates glutamine synthetase (central vein); green, vector-expressed EGFP; and blue, DAPI (nuclei). Scale bars, 500  $\mu$ m. (G-H) Quantification of (G) AAV vector genomes per diploid cell and (H) mg of GFP per mg of total protein in murine livers transduced with indicated vectors ( $7.5 \times 10^{10}$  vg / mouse), n.d.: not detected. Data are mean  $\pm$  SD.

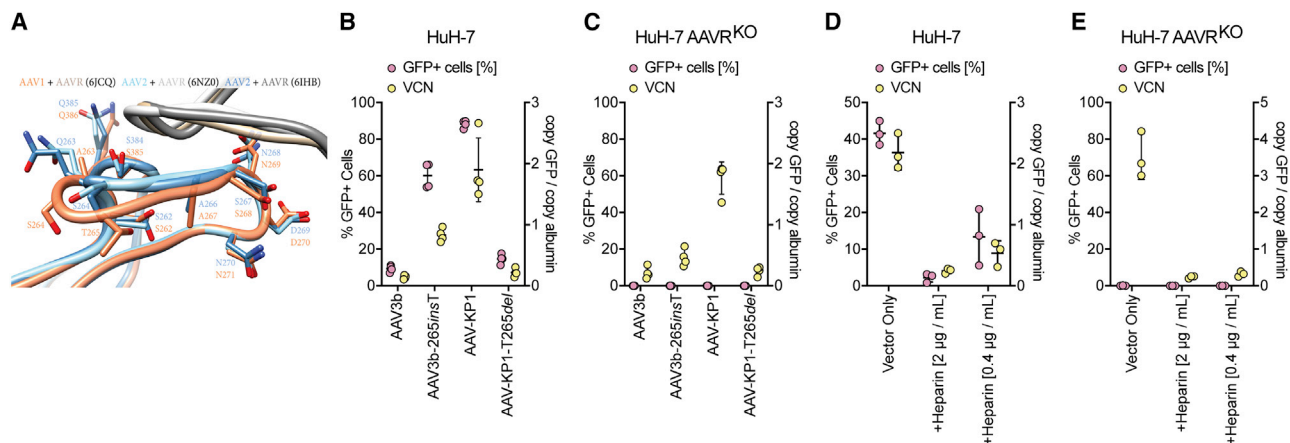


**Figure 6. AAVR is an essential host factor for AAV3b-265insT and AAV-KP1 functional transduction of HuH-7 cells**

(A) Alignment of the AAV/AAVR interface in three structures of AAV in complex with AAVR, one involving AAV1 (orange, AAV1; tan, AAVR; PDB: 6JCQ) and two with AAV2 (light blue, AAV2; light gray AAVR; PDB: 6NZO; and dark blue, AAV2; dark gray, AAVR; PDB: 6IHB). Comparison of AAV1 with AAV2 at the site of the T265 insertion in AAV1 shows that this mutation induces a local deformation of S264 and T264 relative to AAV2 S264, but most downstream residues (S267/268, N268/269, D269/270, N270/271), as well as those at the interface (Q386/286, S384/385), share similar positions. (B and C) Physical transduction (vector copy number) and functional transduction (percentage of GFP<sup>+</sup> cells) of AAV3b and AAV-KP1 variants on wild-type and AAVR KO HuH-7 cells, at multiplicity of transduction (MOT) of 1,000 vg/cell. (D and E) Heparin competition assay. Physical transduction (vector copy number) and functional transduction (percentage of GFP<sup>+</sup> cells) of AAV-KP1 on naive and AAVR KO HuH-7 cells, at MOT of 500 vg/cell. When indicated, soluble heparin was supplemented in the media prior to transduction. Data are mean  $\pm$  SD.

cells that was accompanied by a reduction of vector uptake (Figure 6D). In the presence of soluble heparin, we also observed a matched reduction in vector uptake of AAV-KP1 in HuH-7 AAVR<sup>KO</sup> cells (Figure 6E).

#### Functional deficiency in murine transduction of HSPG de-targeted AAV-LK03 is independent of attachment

Numerous studies have reported that HSPG binding is essential for murine liver transduction of clade C AAV variants, such as AAV2 and AAV3b, given the observed drop in the transduction of this organ with HSPG-ablated variants.<sup>20,21</sup> Intriguingly, our data fit a model that explores a post-attachment deficiency mechanism for clade B/C variants. To study this model, we generated three variants of AAV-LK03,<sup>6</sup> a human tropic capsid with high sequence identity to AAV3b. These included an HSPG de-targeted variant (AAV-LK03-R594G, Table 1) and two murine surrogates with the inclusion of 265insT in the parental AAV-LK03 and its HSPG de-targeted variant. As shown in Figures 7A and 7B and the upper panels of Figure 7C, the residual murine functional transduction of AAV-LK03 was indeed further reduced with the introduction of the HSPG de-targeting R594G amino acid change, which is consistent with the existing literature on the HSPG binding.<sup>20,21</sup> Nevertheless, the introduction of 265T insertion reveals a more comprehensive view of the function of HSPG interaction for AAV-LK03. As shown in Figures 7A and 7B, the 265T insertion substantially increased the ability of AAV-LK03 to transduce the murine liver, for both the prototypical AAV-LK03 (HSPG binder) and its HSPG de-targeted variant, although their lobule biodistribution was markedly different (Figure 7C). Given that the 265T insertion appears to have minimal impact on the HSPG attachment (Table 1), the murine surrogate of

AAV-LK03 displays a marked periportal profile, consistent with high HSPG binding and limited distribution within the hepatic lobule (Figure 7C, lower left panel). This phenotype is lost in the HSPG-de-targeted variant (Figure 7C, lower right panel). Given that both HSPG de-targeted AAV-LK03 variants (with/without 265T) share the same attachment properties, it is reasonable to hypothesize that they also share a similar liver lobule biodistribution. Thus, the substantial change in transduction arises, with most probability, from a post-attachment step, suggesting that successful interaction with either a receptor or an essential host factor, and not HSPG, is the crucial limiting step for successful murine transduction of AAV-LK03-R594G.

To study the effect of the 265T insertion on biodistribution, we used the HSPG-de-targeted AAV-LK03 variants to package AAV cassette encoding EGFP under the control of the ubiquitous human cytomegalovirus (CMV) promoter. We injected  $1 \times 10^{11}$  vg of each vector per mouse in a cohort of three mice per group and evaluated vector biodistribution across tissues (Figure 7D). As expected based on the data discussed earlier, we observed a substantial increase in murine liver entry for the variant harboring the insertion (~20-fold increase in copy number). Although the effect on the peripheral organs was almost negligible in comparison to the liver, we observed a drop in vector copy number per diploid genome in all the organs tested for the variant harboring 265insT. While this could suggest decreased transduction of the other organs, based on the substantial increase of vector entry into hepatocytes (Figures 7E and 7F), we hypothesize that the observed drop in transduction of other organs results from a liver-driven decrease in the availability of free vectors in the blood.

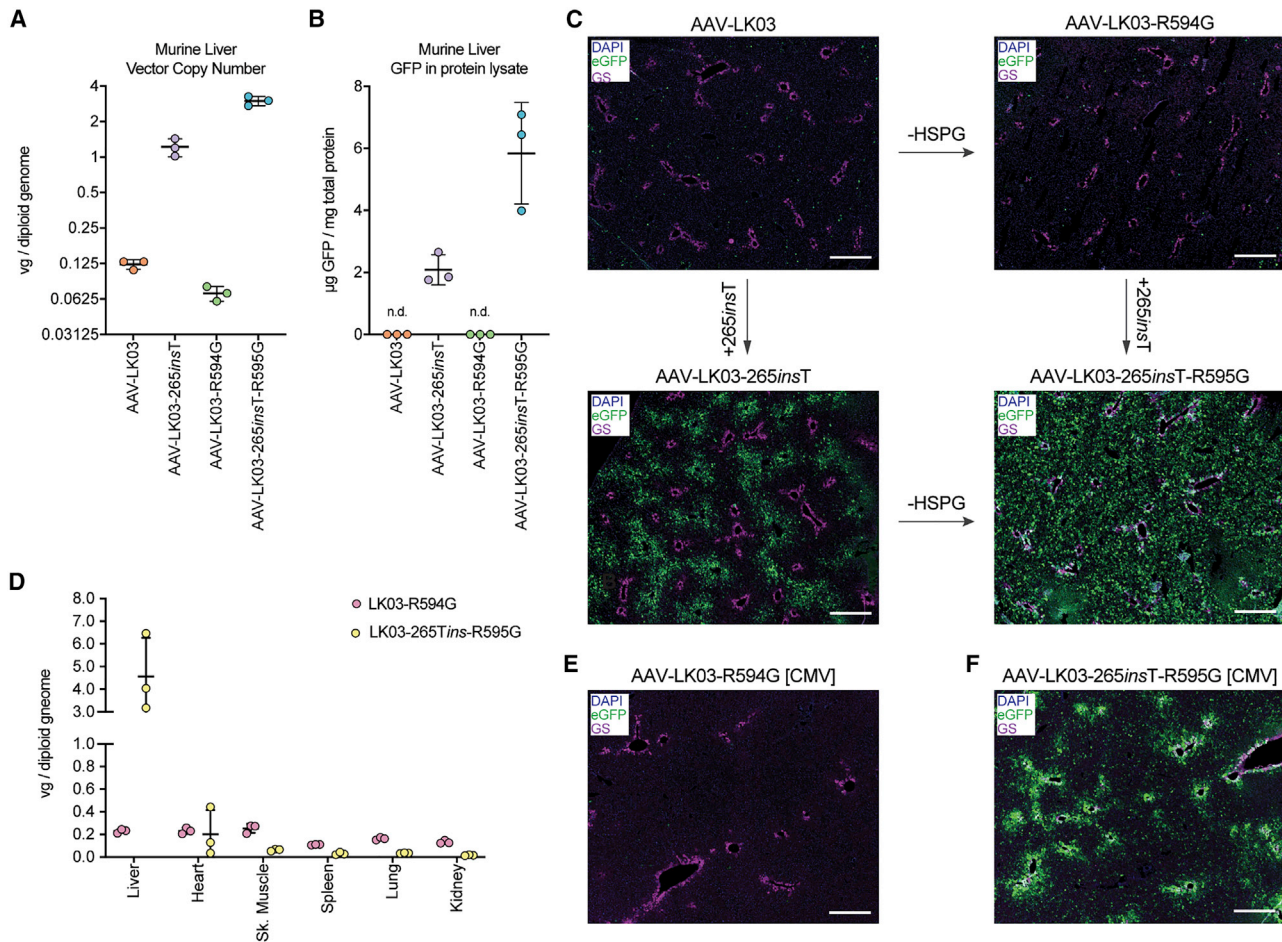


**Figure 7. *In vivo* comparison of AAV-LK03 variants in non-engrafted FRG mice**

All data are representative of  $n = 3$  mice per tested vector. AAV-LK03 variants are divided according to the HSPG-binding profile (HSPG+/-) and presence/absence of 265insT. (A and B) Quantification of (A) AAV vector genomes per diploid cell, and (B)  $\mu\text{g}$  of GFP per mg of protein in murine livers transduced with indicated vectors ( $7.5 \times 10^{10}$  vg/mouse). Data are mean  $\pm$  SD. (C) Representative immunofluorescence analysis of FRG mice livers transduced with the indicated AAV-LK03 variants. Purple indicates glutamine synthetase (central vein); green, vector-expressed EGFP; and blue, DAPI (nuclei). Scale bars, 500  $\mu\text{m}$ . (D) Quantification of AAV vector genomes per diploid genome in the liver, heart, skeletal muscle, spleen, lung, and kidney of mice transduced with indicated vectors (dose of  $1 \times 10^{11}$  vg/mouse). Data are mean  $\pm$  SD (E and F) Representative immunofluorescence analysis of liver tissue of FRG mice transduced with the indicated AAV-LK03 variants encoding a CMV-GFP transgene. Purple indicates glutamine synthetase (central vein); green, vector-expressed EGFP; and blue, DAPI (nuclei). Scale bars, 500  $\mu\text{m}$ .

## DISCUSSION

AAV-KP1 was selected in an *in vitro* screen of a DNA family shuffled library constructed from 18 parental AAV sequences.<sup>13</sup> Thus, each region of this bioengineered capsid can be mapped to a specific AAV variant, or variants, from which it originated (Figure 2G). The closest parental capsid to AAV-KP1 is the prototypical AAV3b (57 aa differences). In this work, we took advantage of domain swapping strategies to identify the insertion of a threonine at position 265 as a key residue enabling successful transduction of murine liver for AAV-KP1. Importantly, this insertion greatly improved the ability of AAV3b (Figure 3A), and other clade B and clade C AAV variants (Figure 5C), to transduce murine hepatocytes. This effect was

so strong that it shifted the preferential transduction of AAV variants harboring the insertion from human to murine hepatocytes in the chimeric hFRG model (Figures 5D and 5E). The effect appears to be independent of HSPG attachment and would be more consistent with a differential engagement of AAV with murine and human receptors essential for cell entry or with an improved interaction with an essential host factor for functional AAV transduction. At this stage, we cannot rule out the possibility that vector genomes lacking the 265insT mutation are rapidly degraded in murine hepatocytes, which would coincide with the observed lower vector copy number per cell. Importantly, we observed a marked increase in genome transcription for the AAV3b-like variants harboring this

particular insertion, in both murine liver and hepatocytes (Figures 5D and 5E).

Our unbiased expression analysis between AAV3b and AAV-KP1 in the murine liver converged with previous and pioneer domain swapping studies between AAV1 and AAV2.<sup>22</sup> As mentioned earlier, given the DNA family shuffled nature of AAV-KP1, it is possible to map the origin of 265T to AAV1. In 2006, Hauck et al.<sup>22</sup> described the generation of a hybrid AAV2 variant (AAV-221-IV) by incorporating 9 aa from AAV1 into AAV2. The insertion of the threonine at position 265 was one of the changes. This AAV2 variant was described to maintain AAV2's heparin-binding profile and to achieve murine muscle transduction similar to that of AAV1.<sup>22</sup>

A few years later, in 2012, the Samulski lab<sup>23</sup> derived a chimeric variant designated AAV2.5 using a rational design strategy. This variant was created by incorporating 5 aa from AAV1 into the AAV2 background (Q263A, N705A, V708A, and T716N, and insertion of 265T, AAV2 numbering). AAV2.5 was found to maintain AAV2's heparin-binding function, to transduce murine skeletal muscle with higher efficiency than AAV2 and to evade neutralization by the A20 antibody. This variant was subsequently used in a phase I gene therapy trial for Duchenne muscular dystrophy; however, it did not lead to high transgene expression from primary human muscle cells.<sup>23</sup> In a follow-up study, AAV2.5 was further dissected to study the relative contribution of the five mutations.<sup>24</sup> The authors showed that the transduction level in skeletal muscle of AAV2-265insT (threonine insertion at 265) was comparable to that of AAV2.5.<sup>24</sup> Furthermore, saturation studies at this particular position showed that the increased murine muscle tropism was correlated with the amino acid insertion, resulting in a structural change, and it was not linked to any particular amino acid, which is in agreement with our saturation data (Figure 4).<sup>24</sup> Relevant to this topic is the work by Piacentino et al.,<sup>25</sup> who described a chimeric version of AAV3b with an amino acid insertion of a threonine following amino acid position 264 (265insT, AAV3.1). When injected directly in the gastrocnemius muscle, the authors described a substantial increase in murine muscle transduction in comparison to wild-type AAV3b.<sup>25</sup>

More recently, the Vandenberghe lab (E. Zinn et al., 2020, ASGCT conference) described a liver-on/liver-off toggle, a single point mutation in VR-I that can modulate the liver tropism of AAV variants, including AAV3b. At the time of submission of our study, the work from the Vandenberghe lab had not yet been published. However, it is described in an international patent application (WO 2019/217911 A1).<sup>26</sup> The patent describes position 266 (AAV-Anc80-L65 numbering) to be an important determinant of liver transduction. More specifically, the original glycine residue at 266 has been described as liver-enhancing, whereas an alanine substitution at the same position has been shown to reduce liver tropism.<sup>26</sup> When it comes to AAV3b, an A266G substitution was suggested as potentially liver enhancing (liver-on). However, we found this substitution to be detrimental for the already weak murine performing AAV3b (Figure S2). In an alternative alignment, a glycine inser-

tion in AAV-Anc80-L65 appears more consistent with the 265insT described throughout this manuscript (Figure S3). In fact, when tested in naive male FRG mice, we found this particular insertion (AAV3b-265insG) to significantly enhance performance of AAV3b in the murine liver (Figure 4G). This suggests that the mentioned liver toggle would be dependent on the AAV variant presenting an insertion following amino acid position 264, at least for clade B and clade C variants. In fact, this variant (AAV3b-265insG) was reported as liver enhancing on the same patent specification (WO 2019/217911 A1).

An exquisite work that involves AAV1's T265 and is relevant to this study was published in 2018 by Albright et al.<sup>27</sup> from the Asokan group. Using domain swapping between AAV1 and AAV-rh.10, the authors mapped the capsid structural determinants that enable AAVrh.10 to cross the blood-brain barrier (BBB).<sup>27</sup> This swapping approach allowed the authors to rationally design an AAV1 variant able to cross the BBB. This AAV1 variant, named AAV1RX, harbored 8 aa residues from AAVrh.10. Among these changes, AAV1's threonine 265 was substituted with a serine, and, perhaps more importantly, a glycine was inserted following AAV1's position 266 (267G). These changes in VR-I were reported to increase transduction of the brain and reduce liver transduction of AAV1 through an unknown mechanism.<sup>27</sup>

Overall, the existing literature describing modifications of AAV VR-I residues appears to be in agreement across laboratories and suggests that the substantial changes observed in murine functional transduction are independent of cell attachment and more consistent with the implication of VR-I in protein-mediated entry mechanisms or interaction with essential host factors. Pivotal for the work and discussion presented herein are the observations from Chapman and colleagues,<sup>19</sup> which stated that glycans should only be considered as attachment factors, rather than primary receptors, and that productive cell entry of AAV depends on interactions with different protein receptors that have the properties of classical viral entry receptors.<sup>19</sup> Interestingly, AAV-KP1, AAV3b, and their related 265Tdel and 265insT variants appear to be dependent on AAVR for a functional transduction (transgene expression, Figure 6). However, we observed vector entry even in the absence of AAVR, at the dose (multiplicity of transduction [MOT]) tested. This is not in contradiction to published data, given that only functional tests, specifically luciferase expression assays, were performed.<sup>17</sup> However, our data are more consistent with a model where AAVR plays a similar role in AAV transduction to the Golgi calcium transport pump SPCA1,<sup>28</sup> which has recently been described as an essential host factor for intracellular trafficking. Productive intracellular trafficking would then lead to capsid conformational changes that support efficient transduction.<sup>28</sup>

We think that our *in vivo* study with the AAV-LK03 mutants (Figures 7A–7C) can shed some light on the long-lasting confusion around AAV transduction when it comes to the lack of distinction between cell attachment and cell entry.<sup>19</sup> AAV-LK03, which, similar to AAV-KP1, shares the key arginine for HSPG binding from AAV3b

(R594), functions poorly in the murine liver when assessed using single-stranded AAV vector. The reduction of heparin affinity with the introduction of R594G in AAV-LK03 appears to be detrimental and causes a further reduction in murine liver transduction (Figures 7A–7C). By focusing solely on HSPG affinity, one could conclude that HSPG attachment plays an important role in transduction. However, a broader view reveals that this is not the case. With the introduction of the 265T insertion in AAV-LK03, it seems appreciable that R594G only modifies the biodistribution of AAV-LK03 in the murine liver lobule (Figure 7C). Given its strong HSPG binding, AAV-LK03 (such as AAV-KP1) presents a marked periportal performance. By unlocking (reducing) the attachment, it is possible to generate a variant with increased distribution across the hepatic lobule (Figures 3B and 7C). This could be of relevance in non-human primates or even for human studies, where an accumulation of vector in the periportal area could lead to cell exhaustion or toxicity. Further studies in non-human primates will be required to prove or refute this hypothesis.

In summary, the systematic comparison between AAV-KP1 and AAV3b allowed us to identify a threonine insertion at position 265 within VR-I as the key residue that confers murine transduction to human-derived clade B (AAV2-like) and clade C (AAV3b-like) variants. We think that this insertion could be used to generate phylogenetically related surrogates of otherwise human liver tropic (and murine dysfunctional) AAV variants in support of toxicology and dosing studies in the murine liver model.

## MATERIALS AND METHODS

### Mouse studies

All animal care and experimental procedures were approved by the joint Children's Medical Research Institute (CMRI) and The Children's Hospital at Westmead Animal Care and Ethics Committee. CMRI's established FRG<sup>15</sup> mouse colony was used to breed recipient animals. FRG mice were housed in individually ventilated cages with 2-(2-nitro-4-trifluoro-methylbenzoyl)-1,3-cyclohexanedione (NTBC) supplemented in drinking water (8 mg/mL). FRG mice, 6 to 8 weeks old, were engrafted with human hepatocytes (Lonza, Basel, Switzerland) as described previously. hFRG mice were placed on 10% NTBC prior to transduction with vectors and were maintained on 10% NTBC until harvest. Detailed information on all hFRG mice used in the study, including individual estimated repopulation, can be found in Table S2. Mice were randomly selected and injected intravenously (lateral tail vein) with the indicated vectors at a dose of  $5 \times 10^{10}$  vg/vector for NGS comparison, at a dose of  $2 \times 10^{11}$  vg/vector for immunofluorescence studies on hFRG, and at a dose of  $7.5 \times 10^{11}$  vg/vector for immunofluorescence studies on naive male FRG mice (10–12 weeks old). Mice were euthanized by CO<sub>2</sub> inhalation 2 weeks after transduction for immunohistochemistry and 1 week after transduction for barcoded NGS analysis. Hepatocytes for flow cytometry analysis were obtained by collagenase perfusion of the liver as recently published.<sup>5,29</sup> In order to reduce the presence of endothelial cells, they were labeled and excluded with a CD31 antibody (Abcam, ab28364).

### Immunofluorescence analysis of mouse livers

Mouse livers were processed as described recently with no modifications.<sup>5</sup> Briefly, mouse livers fixed with 4% (w/v) paraformaldehyde, cryo-protected in 10%–30% (w/v) sucrose before freezing in O.C.T. (Tissue-Tek; Sakura Finetek USA, Torrance, CA, USA). Frozen liver sections (5  $\mu$ m) were permeabilized in  $-20^{\circ}\text{C}$  methanol, then at room temperature in 0.1% Triton X-100, and then reacted with anti-human GAPDH antibody (Abcam, clone EPR6256, catalog no. ab215227), Alexa Fluor 647, and DAPI (Invitrogen, D1306) at 0.08 ng/mL. After immunolabeling, the images were captured and analyzed on a Zeiss Axio Imager.M1 using ZEN 2 software.

### Culture and immunofluorescence analysis of HuH-7 cells

Cells were cultured in Dulbecco's modified Eagle's medium (DMEM) (Gibco, 11965-092) supplemented with 100 U/mL penicillin/100  $\mu$ g/mL streptomycin (Sigma-Aldrich, P4458) and 10% fetal bovine serum (FBS) (Sigma-Aldrich, F9423 [500 mL], lot no. 16K598) and non-essential amino acids (Gibco, 11140-050). Cells were passaged using TrypLE express enzyme (Gibco, 12604-21). For transduction studies, cells were plated into 24-well plates in complete DMEM at  $1 \times 10^5$  cells per well and incubated overnight in a tissue-culture incubator at  $37^{\circ}\text{C}/5\% \text{CO}_2$ . 16 h later, the vector stock was added to cells (at the indicated vg copies/cell). The heparin competition assay was performed as described previously.<sup>4</sup> For immunofluorescence, cells were seeded overnight on coverslips in 24-well plates at a density of  $5 \times 10^4$  cells/well and allowed to adhere overnight. After  $1 \times$  PBS washes, the cells were fixed in 4% paraformaldehyde, permeabilized with 0.2% Triton X-100, and blocked in 10% normal donkey serum diluted in  $1 \times$  PBS. Cells were reacted with anti-AAVR antibody (Abcam, ab105385) at 1:100, anti-giantin antibody (BioLegend, 908701)/Alexa Fluor 488 at 1:500, and DAPI (Invitrogen, D1306) at 0.08 ng/mL. After immunolabeling, the images were captured and analyzed on a LSM 800-Airyscan microscope using ZEN Black software.

### AAV transgene constructs

AAV transgene constructs and capsid variants were cloned using standard molecular biological techniques. All of the vectors used in the study contain AAV2 inverted terminal repeat (ITR) sequences. The single-stranded AAV construct pLSP1-EGFP-WPRE-BGHpA, which encodes EGFP under the transcriptional control of a heterologous promoter containing one copy of the *SERPINA1* (hAAT) promoter and two copies of the *APOE* enhancer element, has been previously reported. Barcoded versions of this construct were used for the *in vivo* NGS-barcoded comparisons as published recently.<sup>4</sup>

### AAV vector packaging and viral production

AAV constructs were packaged into AAV capsids using HEK293 cells and a helper-virus-free system as previously described.<sup>30</sup> The plasmid encoding for AAV-KP1 was a gift from Prof. Mark Kay. All vectors/viruses were purified using iodixanol gradient ultracentrifugation as previously described.<sup>31</sup> AAV preparations were titered by droplet digital PCR (ddPCR) using EGFP-specific primers EGFP-forward/reverse (For/Rev) (Table S3).

### Barcode amplification, NGS, and distribution analysis

The region surrounding the 6-mer barcode was amplified with Q5 with Q5 high-fidelity DNA polymerase (NEB, catalog no. M0491L) using BC\_F and BC\_R primers. Amplicon NGS was performed as described before with no modifications.<sup>5</sup> All codes used to count barcodes in paired-end Illumina reads from PCR amplicons are available on Code Ocean (<https://doi.org/10.24433/CO.7176285.v1>)

### Heparin binding assay

The heparin affinity of various AAV vector variants was determined as recently published with no modifications.<sup>5</sup> A 1-mL HiTrap heparin HP column (GE Healthcare, catalog no. 1704601, lot no. 10276193) was used on an ÄKTA pure 25 M2 (GE Healthcare) fast protein liquid chromatography system.

### AAV and AAVR structural visualizations

To visualize the AAV-AAVR interface, RCSB PDB: 6JCQ, 6NZ0 and 6IHB were downloaded. These structures were visualized in Chimera<sup>32</sup> and aligned using MatchMaker<sup>33</sup> (using chain A). To show the location of the 265T mutation relative to the HSPG binding domain, RCSB PDB: 3KIC (biological assembly 1) was downloaded and the surface rendered with ChimeraX.

### Saturation AAV3b-265inxX library

The saturation library described in Figure 4 was built following the “small-intelligent” method previously described by Tang and colleagues.<sup>34</sup> Briefly, a plasmid encoding for the full AAV3b *cap* region flanked with *Swa*I and *Nsi*I flanking sites was amplified with a mixture of four forward primers and one common reverse primer, allowing self-assembly of the PCR product via Gibson assembly, as shown in detail in Figure S4. The forward primers encoded for codons corresponding to the insertion of 12 aa (NDT codon), 6 aa (VMA codon), 1 aa (TGG codon), and 1 aa (ATG codon), and thus they were mixed at a 12:6:1:1 ratio for the PCR reaction. The PCR reaction was partially digested with *Dpn*I (NEB) to maintain the desired degree of “background” AAV3b (Figure 4A, no insertion). The full *cap* was then excised using *Swa*I and *Nsi*I (NEB) and cloned into the functional transduction platform with regular ligation at 16°C with T4 DNA ligase (NEB, catalog no.M0202).

### HuH-7 AAVR<sup>KO</sup> cell line generation

The plasmid designed for expression of single guide RNA (sgRNA) and wild-type SpCas9 carrying puromycin resistance gene was obtained from Addgene (catalog no. 62988). To express gRNA, single-stranded oligonucleotides (Sigma) containing the guide sequence of the gRNAs were annealed, phosphorylated, and ligated into the *Bbs*I site of pSpCas9(BB)-2A-Puro backbone. Two gRNAs were used to generate large deletions. Both exon 4 and exon 13 were targeted in the AAVR gene. Relevant primers can be found in Table S3. HuH-7 cells were transfected using Amaxa 4D nucleofection systems (Lonza) according to the manufacturer’s instructions using SF transfection and program FF-138. Twenty-four hours post-transfection cells were selected with puromycin (1 µg/mL) (Thermo Fisher Scientific) for 48 h. After selection and colony expansion, single

clones were selected by limited dilution and grown in 96-well plates. To determine the genotype of each clone, Sanger sequencing was performed on PCR products amplified from genomic DNA spanning the gRNA target sites. The selected clone harbored one large deletion and one nucleotide insertion as schematized in Figure S5.

### SUPPLEMENTAL INFORMATION

Supplemental information can be found online at <https://doi.org/10.1016/j.omtm.2021.04.010>.

### ACKNOWLEDGMENTS

We thank the CMRI Vector and Genome Engineering Facility (VGEF), with special thanks to Maddison Knight and Predrag Kalajdzic, for help in vector preparation and for the generation of the HuH-7 AAVR<sup>KO</sup> cell line. We also thank the Cytometry Facility of the Westmead Institute for Medical Research for help with the sorting of murine hepatocytes. We also would like to thank all the members of the CMRI Bioresources, with special thanks to S. Dimech. This work was supported by project grants from the Australian National Health and Medical Research Council (NHMRC) (APP1108311, APP1156431, and APP1161583) to L.L. and I.E.A. and the Paediatric Paediatric Precision Medicine Program (PPM1 K5116/RD274) to L.L., as well as funding from LogicBio Therapeutics. L.L. was also supported by research grants from the Department of Science and Higher Education of Ministry of National Defense, Republic of Poland (“Kościuszko” k/10/8047/DNiSW/T – WIHE/3) and from the National Science Centre, Republic of Poland (OPUS 13) (UMO-2017/25/B/NZ1/02790).

### AUTHOR CONTRIBUTIONS

Conceptualization, M.C.-C. and L.L.; methodology, M.C.-C., R.G.N., and E.Z.; software, S.S. and L.O.W.W.; investigation, M.C.-C., R.G.N., S.H.Y.L., G.B., E.Z., and C.L.; writing – original draft, M.C.-C. and L.L.; writing – review & editing, M.C.-C., S.S., and L.L.; funding acquisition, I.E.A. and L.L.; visualization, M.C.-C. and M.D.; supervision: M.C.-C., I.E.A., and L.L.

### DECLARATION OF INTERESTS

M.C.-C., I.E.A., and L.L. are inventors on patent applications filed by Children’s Medical Research Institute related to AAV capsid sequences and *in vivo* function of novel AAV variants. L.L. is a co-founder and scientific advisor of LogicBio Therapeutics. L.L. and I.E.A. are co-founders of Exigen Biotherapeutics. L.L. has a sponsored research agreement with LogicBio Therapeutics. M.C.-C., I.E.A. and L.L. have intellectual property (IP) licensed to biopharmaceutical companies. L.L. and I.A.E. have consulted on technologies addressed in this paper. L.L. and I.A.E. have stock and/or equity in companies with technology broadly related to this paper. The remaining authors declare no competing interest.

### REFERENCES

1. Kattenhorn, L.M., Tipper, C.H., Stoica, L., Geraghty, D.S., Wright, T.L., Clark, K.R., and Wadsworth, S.C. (2016). Adeno-associated virus gene therapy for liver disease. *Hum. Gene Ther.* 27, 947–961.

2. Nathwani, A.C. (2019). Gene therapy for hemophilia. *Hematology (Am. Soc. Hematol. Educ. Program)* 2019, 1–8.
3. Paulk, N.K., Pekrun, K., Zhu, E., Nygaard, S., Li, B., Xu, J., Chu, K., Leborgne, C., Dane, A.P., Haft, A., et al. (2018). Bioengineered AAV capsids with combined high human liver transduction *in vivo* and unique humoral seroreactivity. *Mol. Ther.* 26, 289–303.
4. Cabanes-Creus, M., Westhaus, A., Navarro, R.G., Baltazar, G., Zhu, E., Amaya, A.K., Liao, S.H.Y., Scott, S., Sallard, E., Dilworth, K.L., et al. (2020). Attenuation of heparan sulfate proteoglycan binding enhances *in vivo* transduction of human primary hepatocytes with AAV2. *Mol. Ther. Methods Clin. Dev.* 17, 1139–1154.
5. Cabanes-Creus, M., Hallwirth, C.V., Westhaus, A., Ng, B.H., Liao, S.H.Y., Zhu, E., Navarro, R.G., Baltazar, G., Drouyer, M., Scott, S., et al. (2020). Restoring the natural tropism of AAV2 vectors for human liver. *Sci. Transl. Med.* 12, eaba3312.
6. Lisowski, L., Dane, A.P., Chu, K., Zhang, Y., Cunningham, S.C., Wilson, E.M., Nygaard, S., Grompe, M., Alexander, I.E., and Kay, M.A. (2014). Selection and evaluation of clinically relevant AAV variants in a xenograft liver model. *Nature* 506, 382–386.
7. Zou, C., Vercauteren, K.O.A., Michailidis, E., Kabbani, M., Zolotukhin, I., Quirk, C., Chiriboga, L., Yazicioglu, M., Anguela, X.M., Meuleman, P., et al. (2020). Experimental variables that affect human hepatocyte AAV transduction in liver chimeric mice. *Mol. Ther. Methods Clin. Dev.* 18, 189–198.
8. Gao, G., Vandenberghe, L.H., Alvira, M.R., Lu, Y., Calcedo, R., Zhou, X., and Wilson, J.M. (2004). Clades of adeno-associated viruses are widely disseminated in human tissues. *J. Virol.* 78, 6381–6388.
9. Dane, A.P., Wowro, S.J., Cunningham, S.C., and Alexander, I.E. (2013). Comparison of gene transfer to the murine liver following intraperitoneal and intraportal delivery of hepatotropic AAV pseudo-serotypes. *Gene Ther.* 20, 460–464.
10. Westhaus, A., Cabanes-Creus, M., Rybicki, A., Baltazar, G., Navarro, R.G., Zhu, E., Drouyer, M., Knight, M., Albu, R.F., Ng, B.H., et al. (2020). High-throughput *in vitro*, *ex vivo*, and *in vivo* screen of adeno-associated virus vectors based on physical and functional transduction. *Hum. Gene Ther.* 31, 575–589.
11. Bell, P., Wang, L., Gao, G., Haskins, M.E., Tarantal, A.F., McCarter, R.J., Zhu, Y., Yu, H., and Wilson, J.M. (2011). Inverse zonation of hepatocyte transduction with AAV vectors between mice and non-human primates. *Mol. Genet. Metab.* 104, 395–403.
12. Grimm, D., Lee, J.S., Wang, L., Desai, T., Akache, B., Storm, T.A., and Kay, M.A. (2008). *In vitro* and *in vivo* gene therapy vector evolution via multispecies interbreeding and retargeting of adeno-associated viruses. *J. Virol.* 82, 5887–5911.
13. Pekrun, K., De Alencastro, G., Luo, Q.J., Liu, J., Kim, Y., Nygaard, S., Galivo, F., Zhang, F., Song, R., Tiffany, M.R., et al. (2019). Using a barcoded AAV capsid library to select for clinically relevant gene therapy vectors. *JCI Insight* 4, e131610.
14. Lerch, T.F., and Chapman, M.S. (2012). Identification of the heparin binding site on adeno-associated virus serotype 3B (AAV-3B). *Virology* 423, 6–13.
15. Azuma, H., Paulk, N., Ranade, A., Dorrell, C., Al-Dhalimy, M., Ellis, E., Strom, S., Kay, M.A., Finegold, M., and Grompe, M. (2007). Robust expansion of human hepatocytes in *Fah<sup>-/-</sup>/Rag2<sup>-/-</sup>/Il2rg<sup>-/-</sup>* mice. *Nat. Biotechnol.* 25, 903–910.
16. Drouin, L.M., and Agbandje-McKenna, M. (2013). Adeno-associated virus structural biology as a tool in vector development. *Future Virol.* 8, 1183–1199.
17. Pillay, S., Meyer, N.L., Puschnik, A.S., Davulcu, O., Diep, J., Ishikawa, Y., Jae, L.T., Wosen, J.E., Nagamine, C.M., Chapman, M.S., and Carette, J.E. (2016). An essential receptor for adeno-associated virus infection. *Nature* 530, 108–112.
18. Zhang, R., Cao, L., Cui, M., Sun, Z., Hu, M., Zhang, R., Stuart, W., Zhao, X., Yang, Z., Li, X., et al. (2019). Adeno-associated virus 2 bound to its cellular receptor AAVR. *Nat. Microbiol.* 4, 675–682.
19. Meyer, N.L., Hu, G., Davulcu, O., Xie, Q., Noble, A.J., Yoshioka, C., Gingerich, D.S., Trzynka, A., David, L., Stagg, S.M., and Chapman, M.S. (2019). Structure of the gene therapy vector, adeno-associated virus with its cell receptor, AAVR. *eLife* 8, e44707.
20. Gorbatyuk, O.S., Warrington, K.H., Jr., Gorbatyuk, M.S., Zolotukhin, I., Lewin, A.S., and Muzyczka, N. (2019). Biodistribution of adeno-associated virus type 2 with mutations in the capsid that contribute to heparan sulfate proteoglycan binding. *Virus Res.* 274, 197771.
21. Ogden, P.J., Kelsic, E.D., Sinai, S., and Church, G.M. (2019). Comprehensive AAV capsid fitness landscape reveals a viral gene and enables machine-guided design. *Science* 366, 1139–1143.
22. Hauck, B., Xu, R.R., Xie, J., Wu, W., Ding, Q., Sipler, M., Wang, H., Chen, L., Wright, J.F., and Xiao, W. (2006). Efficient AAV1-AAV2 hybrid vector for gene therapy of hemophilia. *Hum. Gene Ther.* 17, 46–54.
23. Bowles, D.E., McPhee, S.W., Li, C., Gray, S.J., Samulski, J.J., Camp, A.S., Li, J., Wang, B., Monahan, P.E., Rabinowitz, J.E., et al. (2012). Phase 1 gene therapy for Duchenne muscular dystrophy using a translational optimized AAV vector. *Mol. Ther.* 20, 443–455.
24. Li, C., Diprimio, N., Bowles, D.E., Hirsch, M.L., Monahan, P.E., Asokan, A., Rabinowitz, J., Agbandje-McKenna, M., and Samulski, R.J. (2012). Single amino acid modification of adeno-associated virus capsid changes transduction and humoral immune profiles. *J. Virol.* 86, 7752–7759.
25. Piacentino, V., 3rd, Milano, C.A., Bolanos, M., Schroder, J., Messina, E., Cockrell, A.S., Jones, E., Krol, A., Bursac, N., Mao, L., et al. (2012). X-linked inhibitor of apoptosis protein-mediated attenuation of apoptosis, using a novel cardiac-enhanced adeno-associated viral vector. *Hum. Gene Ther.* 23, 635–646.
26. Vandenberghe, L.H., Schmit, P., Tipper, C., Unzu, C., and Zinn, E. (2018). Liver-specific tropism of adeno-associated viruses. International patent application publication WO 2019/217911 A1, filed May 10, 2019, and published November 14, 2019.
27. Albright, B.H., Storey, C.M., Murlidharan, G., Castellanos Rivera, R.M., Berry, G.E., Madigan, V.J., and Asokan, A. (2018). Mapping the structural determinants required for AAVrh.10 transport across the blood-brain barrier. *Mol. Ther.* 26, 510–523.
28. Madigan, V.J., Berry, G.E., Tyson, T.O., Nardone-White, D., Ark, J., Elmore, Z.C., Murlidharan, G., Vincent, H.A., and Asokan, A. (2020). The Golgi calcium ATPase pump plays an essential role in adeno-associated virus trafficking and transduction. *J. Virol.* 94, e01604-20.
29. Cabanes-Creus, M. (2020). Isolation of human hepatocytes by collagenase perfusion. Bio-protocol, <https://bio-protocol.org/prep532>.
30. Xiao, X., Li, J., and Samulski, R.J. (1998). Production of high-titer recombinant adeno-associated virus vectors in the absence of helper adenovirus. *J. Virol.* 72, 2224–2232.
31. Khan, I.F., Hirata, R.K., and Russell, D.W. (2011). AAV-mediated gene targeting methods for human cells. *Nat. Protoc.* 6, 482–501.
32. Pettersen, E.F., Goddard, T.D., Huang, C.C., Couch, G.S., Greenblatt, D.M., Meng, E.C., and Ferrin, T.E. (2004). UCSF Chimera—a visualization system for exploratory research and analysis. *J. Comput. Chem.* 25, 1605–1612.
33. Meng, E.C., Pettersen, E.F., Couch, G.S., Huang, C.C., and Ferrin, T.E. (2006). Tools for integrated sequence-structure analysis with UCSF Chimera. *BMC Bioinformatics* 7, 339.
34. Tang, L., Gao, H., Zhu, X., Wang, X., Zhou, M., and Jiang, R. (2012). Construction of “small-intelligent” focused mutagenesis libraries using well-designed combinatorial degenerate primers. *Biotechniques* 52, 149–158.